J. Fluid Mech. (2011), *vol.* 678, *pp.* 221–247. © Cambridge University Press 2011
doi:10.1017/jfm.2011.108

Dynamics of a non-spherical microcapsule with incompressible interface in shear flow

P. M. VLAHOVSKA[1]†, Y.-N. YOUNG[2], G. DANKER[3] AND C. MISBAH[3]

[1]School of Engineering, Brown University, Providence, RI 02912, USA

[2]Department Mathematical Sciences, New Jersey Institute of Technology, Newark, NJ 07102, USA

[3]Laboratoire de Spectrométrie Physique, UMR, 140 avenue de la physique, Université Joseph Fourier and CNRS, 38402 Saint Martin d'Heres, France

(Received 24 April 2010; revised 17 February 2011; accepted 25 February 2011; first published online 18 April 2011)

We study the motion and deformation of a liquid capsule enclosed by a surface-incompressible membrane as a model of red blood cell dynamics in shear flow. Considering a slightly ellipsoidal initial shape, an analytical solution to the creeping-flow equations is obtained as a regular perturbation expansion in the excess area. The analysis takes into account the membrane fluidity, area-incompressibility and resistance to bending. The theory captures the observed transition from tumbling to swinging as the shear rate increases and clarifies the effect of capsule deformability. Near the transition, intermittent behaviour (swinging periodically interrupted by a tumble) is found only if the capsule deforms in the shear plane and does not undergo stretching or compression along the vorticity direction; the intermittency disappears if deformation along the vorticity direction occurs, i.e. if the capsule 'breathes'. We report the phase diagram of capsule motions as a function of viscosity ratio, non-sphericity and dimensionless shear rate.

Key words: capsule/cell dynamics

1. Introduction

Membrane-enclosed particles, such as red blood cells (RBCs) and capsules, exhibit rich dynamics in flow (see for recent reviews Abkarian & Viallat 2008; Guido & Tomaiuolo 2009; Vlahovska, Podgorski & Misbah 2009; Barthes-Biesel 2010). Two classic types of behaviour in steady shear flow are (i) *tank-treading* (TT), in which the capsule shape is steady and the membrane rotates as a tank-tread; the major axis is tilted with respect to the flow direction and the inclination angle remains fixed in time, and (ii) *tumbling* (TB), in which the particle undergoes a periodic flipping motion. Recently, a new type of motion called *swinging* (SW) has been experimentally observed for RBCs (Abkarian, Faivre & Viallat 2007). In this case, the cell's TT is accompanied by small oscillations in the inclination angle. A similar phenomenon has been reported for capsules (Navot 1998; Ramanjuan & Pozrikidis 1998; Walter, Rehage & Leonhard 2001) and drops covered with the adsorbed protein layer (Erni, Fischer & Windhab 2005).

† Email address for correspondence: petia_vlahovska@brown.edu

https://doi.org/10.1017/jfm.2011.108 Published online by Cambridge University Press

Analyses of the SW motion have generated certain controversy. Phenomenological models (Abkarian *et al.* 2007; Skotheim & Secomb 2007; Kessler, Finken & Seifert 2009; Noguchi 2009) based on the theory by Keller & Skalak (1982), which approximates the RBC with an ellipsoid of fixed shape, predicted intermittent behaviour (SW periodically interrupted by a tumble), for which no evidence was found in the numerical simulations (Kessler, Finken & Seifert 2008; Sui *et al.* 2008; Bagchi & Kalluri 2009). The RBC is a deformable particle. Moreover, its membrane can be treated as a visco-elastic incompressible interface: it is made of a lipid bilayer, which behaves as a two-dimensional incompressible fluid, attached to an underlying polymer network, which endows the membrane with shear elasticity. The objective of our work is to develop a rigorous analytical theory that disposes of the assumptions for a fixed ellipsoidal shape and compressible membrane inherent to the studies based on the Keller–Skalak model. Our model builds upon the theories for the dynamics of a vesicle, which is a closed lipid membrane (Misbah 2006; Vlahovska & Gracia 2007), and an initially spherical capsule (Barthes-Biesel 1980; Barthes-Biesel & Rallison 1981) in shear flows. Our theory accounts for the membrane area-incompressibility, shear elasticity and non-spherical rest shape. We assume nearly spherical shape because this simple geometry is amenable to analytical solution. Accordingly, the model provides only qualitative information because the RBC's equilibrium shape is a biconcave disc. However, the analytical solution allows us to take into account all features of the membrane rheology and the results are useful to validate numerical models.

Section 2 formulates the model, § 3 summarizes the theory for fluid membranes (vesicles) and elastic interfaces (initially spherical capsules), and derives the evolution equations for the capsule shape and orientation angle. Section 4 analyses the effects of shear elasticity on capsule dynamics and the SW–TB transition.

2. Problem formulation

Let us consider a capsule with total area A enclosing a fluid of viscosity η^{in} and suspended in a fluid of viscosity η^{ex}. Both interior and exterior fluids are incompressible and Newtonian. The capsule has a characteristic size R_0 defined by the radius of a sphere of the same volume. The non-sphericity of the rest shape is characterized by an excess area

$$\Delta = A/R_0^2 - 4\pi. \tag{2.1}$$

The typical value for a RBC is $\Delta \sim 4$.

We seek to determine the motion and deformation of a capsule that is freely suspended in an unbounded linear shear flow, with velocity $\boldsymbol{v}^{\infty}$ in a reference frame centred on the capsule centre of mass and moving with the capsule:

$$\boldsymbol{v}^{\infty}(\boldsymbol{r}) = \dot{\gamma}\, y \hat{\boldsymbol{x}}, \tag{2.2}$$

where $\dot{\gamma}$ is the strain rate. The problem is sketched in figure 1.

2.1. *Fluid motion and fluid–membrane coupling*

Dynamics of a microcapsule that is freely suspended in an unbounded linear shear flow is a classical problem for which the governing equations are well established (Barthes-Biesel & Rallison 1981; Pozrikidis 2003). The fluid velocity $\boldsymbol{v}^{(\alpha)}$ and pressure $p^{(\alpha)}$ of the interior ('$\alpha = in$') and suspending ('$\alpha = ex$') fluids obey the Stokes equations

https://doi.org/10.1017/jfm.2011.108 Published online by Cambridge University Press

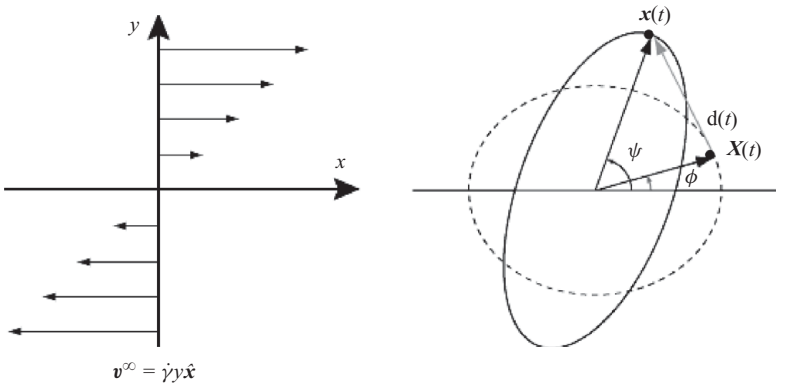


FIGURE 1. Sketch of the flow and capsule configuration. ψ is the inclination angle of the capsule major axis, ϕ is the angle between the flow direction and the material particle in the reference configuration. The time rate of change of the phase angle $\psi - \phi$ is the TT frequency of the membrane.

and the incompressibility condition

$$\nabla \cdot \boldsymbol{T}^{(\alpha)} = -\nabla p^{(\alpha)} + \eta^{(\alpha)} \nabla^2 \boldsymbol{v}^{(\alpha)} = 0, \quad \nabla \cdot \boldsymbol{v}^{(\alpha)} = 0, \tag{2.3}$$

where $\boldsymbol{T}$ is the bulk hydrodynamic stress

$$\boldsymbol{T}^{(\alpha)} = -p^{(\alpha)} \boldsymbol{I} + \eta^{(\alpha)} [\nabla \boldsymbol{v}^{(\alpha)} + (\nabla \boldsymbol{v}^{(\alpha)})^{\dagger}]. \tag{2.4}$$

Here, $\boldsymbol{I}$ denotes the unit tensor and the superscript † denotes transpose. Far away from the capsule, the flow field tends to the unperturbed external flow $\boldsymbol{v}^{ex} \to \boldsymbol{v}^{\infty}$.

At the interface, the velocity is continuous. However, the hydrodynamic stresses undergo a jump, which is balanced by membrane surface forces:

$$\boldsymbol{v}^{in} = \boldsymbol{v}^{ex} = \boldsymbol{v}^{mm}, \quad \boldsymbol{n} \cdot (\boldsymbol{T}^{ex} - \boldsymbol{T}^{in}) = \boldsymbol{\tau}^{mm}, \tag{2.5}$$

where $\boldsymbol{n}$ is the outward unit normal vector. The membrane surface forces $\boldsymbol{\tau}^{mm}$ have an elastic component that depends on the displacement of material particles. The latter is determined from the kinematic condition at the interface:

$$\frac{\partial}{\partial t} \boldsymbol{x}(\boldsymbol{X}, t) = \boldsymbol{v}^{mm}, \tag{2.6}$$

where the material points of the membrane are labelled by their position $\boldsymbol{X}$ in the unstressed (initial) configuration, see figure 1. The simultaneous use of Lagrangian ($\boldsymbol{X}$) and Eulerian ($\boldsymbol{x}$) descriptions for the membrane and fluid motion makes capsule dynamics a non-trivial problem (Barthes-Biesel 1980). For example, at a steady TT state, the deformation at a fixed Eulerian point is constant in time unlike that at a fixed material point because material elements rotate.

2.2. *Mechanics of flexible fluid membranes*

The RBC membrane consists of a lipid bilayer attached to protein scaffold. The lipid bilayer endows the membrane with fluidity, incompressibility and bending rigidity, while the polymer network gives rise to resistance to shearing. Since the membrane thickness (5 nm) is small compared to the cell dimensions (few micrometres), the membrane can be treated as a two-dimensional surface embedded in a three-dimensional space.

https://doi.org/10.1017/jfm.2011.108 Published online by Cambridge University Press

For lipid bilayers in the fluid phase, the lipids are free to move within the monolayer. Therefore, a pure fluid bilayer membrane is infinitely shearable (Dimova *et al.* 2006). However, the polymer network lining the bilayer develops elastic tensions when sheared. Different constitutive laws are commonly used to describe the rheological behaviour of thin membranes (Barthes-Biesel 1991; Pozrikidis 2003). If the capsule deformation is sufficiently small, all interface constitutive relations reduce to a linear stress–strain relation, yielding the two-dimensional equivalent of the Hooke's law (Barthes-Biesel & Rallison 1981; Edwards, Brenner & Wasan 1991)

$$\boldsymbol{\tau}^{\mu} = 2(K_A - \mu)(\nabla_s \cdot \boldsymbol{d})H\boldsymbol{n} - (K_A - \mu)\nabla_s\nabla_s \cdot \boldsymbol{d} - \mu\nabla_s \cdot [\nabla_s \boldsymbol{d} \cdot \boldsymbol{I}_s + \boldsymbol{I}_s \cdot (\nabla_s \boldsymbol{d})^{\dagger}], \quad (2.7)$$

where $\boldsymbol{d}$ is the displacement of a material particle of the membrane from its unstressed position, $\boldsymbol{d} = \boldsymbol{x} - \boldsymbol{X}$, see figure 1, and $H = (1/2)\nabla \cdot \boldsymbol{n}$ is the mean curvature. The surface gradient operator is defined as $\nabla_s = \boldsymbol{I}_s \cdot \nabla$, where the matrix $\boldsymbol{I}_s = \boldsymbol{I} - \boldsymbol{nn}$ represents a surface projection. K_A is the stretch and μ is the shear elastic moduli. For a RBC, $\mu \sim 10^{-6}\,\mathrm{N\,m^{-1}}$ and $K_A \sim 200\,\mathrm{N\,m^{-1}}$ (Guido & Tomaiuolo 2009). We can identify $\alpha_2 = K_A - \mu$ and $\alpha_3 = \mu$ in the notation of Barthes-Biesel & Rallison (1981). For an area-incompressible membrane, the first two terms in (2.7) vanish because $\nabla_s \cdot \boldsymbol{d} = 0$.

The simplest model for the bending stresses is derived from the Helfrich curvature energy (Helfrich 1973; Seifert 1997)

$$\boldsymbol{\tau}^{\kappa} = -\kappa(4H^3 - 4KH + 2\nabla_s^2 H)\boldsymbol{n}, \quad (2.8)$$

where $K = (1/2)[(\nabla \cdot \boldsymbol{n})^2 + \nabla\boldsymbol{n} : \nabla\boldsymbol{n}^{\dagger}]$ is the Gaussian curvature, and κ is the bending modulus.

The bilayer consists of fixed number of lipids, which are optimally packed with fixed area per lipid (under moderate stresses). As a result, an element of the bilayer membrane only deforms but cannot change its area. Under stress, the membrane develops tension (a two-dimensional pressure), which adapts itself to the forces exerted on the membrane in order to keep the local and total area constant (Seifert 1999). In other words, the tension of an incompressible surface is a Lagrange multiplier not a material property like surface tension. The corresponding surface force density is

$$\boldsymbol{\tau}^{\sigma} = 2\sigma H\boldsymbol{n} - \nabla_s\sigma, \quad (2.9)$$

where σ denotes the local membrane tension. This tension can be non-uniform along the interface and varies with forcing.

Following Barthes-Biesel & Rallison (1981), we adopt the Cartesian tensor representation of the equations of membrane mechanics (2.7) because it facilitates the connection with the fluid-dynamics problem. The more commonly used representation in terms of surface curvilinear coordinates is well suited for numerical simulations but makes analytical calculations very cumbersome (Barthes-Biesel 1980).

2.3. *Time scales and dimensionless parameters*

Viscous forces exerted by the extensional component of the flow act to distort the shape on a time scale

$$t_{\dot{\gamma}} = (1 + \lambda)\dot{\gamma}^{-1}, \quad (2.10)$$

where $\lambda = \eta^{in}/\eta^{ex}$ is the viscosity ratio. Several intrinsic relaxation mechanisms oppose the deformation. Bending stresses work to bring the shape back to its preferred curvature state; the corresponding time scale is

$$t_{\kappa} = \frac{(1 + \lambda)\eta^{ex}R_0^3}{\kappa}. \quad (2.11)$$

https://doi.org/10.1017/jfm.2011.108 Published online by Cambridge University Press

Relaxation driven by shear elasticity occurs on a time scale

$$t_\mu = \frac{(1+\lambda)\eta^{ex} R_0}{\mu}. \tag{2.12}$$

The factor $(1+\lambda)$ reflects the fact that the more viscous fluid controls the rate of deformation/relaxation. The strength of these relaxation mechanisms that limit shape deformation by the flow is quantified by the corresponding dimensionless parameters: the bending number

$$\mathscr{B} = \frac{t_\kappa}{t_{\dot\gamma}} = \frac{\eta^{ex}\dot\gamma R_0^3}{\kappa}, \tag{2.13}$$

and the elastic capillary number

$$Ca = \frac{t_\mu}{t_{\dot\gamma}} = \frac{\eta^{ex}\dot\gamma R_0}{\mu}. \tag{2.14}$$

In shear flow, the rotational component of the flow imposes rigid body rotation on a particle; the associated time scale is

$$t_\mathrm{r} = \dot\gamma^{-1}. \tag{2.15}$$

Capsule rotation away from the extensional axis of the imposed flow effectively decreases the effect of straining. The rotation effect becomes important for high-viscosity contrast

$$\lambda = \frac{\eta^{in}}{\eta^{ex}} \approx \frac{t_{\dot\gamma}}{t_\mathrm{r}}. \tag{2.16}$$

The interplay of these time scales leads to the complex dynamics of RBCs, capsules and vesicles. Using the typical values for the material properties of a RBC, we estimate that in a flow with shear rate $\dot\gamma = 1\,\mathrm{s}^{-1}$, $\mathscr{B} \sim 1$, $Ca \sim 10^{-3}$ and the rotation rate $\lambda^{-1} \sim 0.1$.

Henceforth, all quantities are non-dimensionalized using η^{ex}, R_0 and $\dot\gamma$. Accordingly, the time scale is $\dot\gamma^{-1}$, the velocity scale is $\dot\gamma R_0$ and bulk stresses are scaled with $\eta^{ex}\dot\gamma$.

3. Perturbative solution for a nearly spherical shape

In order to solve the problem analytically, we consider a nearly spherical particle shape, i.e. $\Delta \ll 1$. In a coordinate system centred at the capsule, the radial position r_s of the interface can be represented as

$$r_\mathrm{s} = 1 + \varepsilon f(\theta, \varphi, t), \tag{3.1}$$

where f is the deviation of particle shape from a sphere of equivalent volume.

In (3.1), the function f representing the shape depends only on angular coordinates. Thus, it is expanded into series of scalar spherical harmonics Y_{jm} (E 1):

$$f = \sum_{j=2}^{\infty} \sum_{m=-j}^{j} f_{jm} Y_{jm}. \tag{3.2}$$

In the above equation, the summation starts from non-zero $j=2$ because the $j=1$ shape modes correspond to translation of the centre of mass. The constraint on fixed total area serves to relate the amplitude of the shape perturbation f and the excess

https://doi.org/10.1017/jfm.2011.108 Published online by Cambridge University Press

area Δ:

$$\Delta = \int \frac{r_s^2}{\hat{\boldsymbol{r}}\cdot\boldsymbol{n}} \sin\theta \, \mathrm{d}\theta \, \mathrm{d}\varphi - 4\pi = \varepsilon^2 \sum_{jm} \frac{(j+2)(j-1)}{2} f_{jm} f_{jm}^* + O(\varepsilon^3), \tag{3.3}$$

where $\hat{\boldsymbol{r}}$ denotes the unit radial vector and the sum over j starts from 2, $|m| \leqslant j$ and $f_{jm}^* = (-1)^m f_{j-m}$. Equation (3.3) suggests that a suitable choice for the small parameter ε in the case of an ellipsoidal shape ($j = 2$) is

$$\varepsilon = \frac{\sqrt{\Delta}}{2}. \tag{3.4}$$

Notably, the small parameter of the perturbation analysis is a geometric quantity, independent of the flow strength and the membrane physical properties. The choice of ε reflects the different dynamics of an initially non-spherical area-incompressible capsule compared to the initially spherical one. The deformation of the latter is accompanied by changes in area, which are limited by the elastic stiffness of the membrane. In contrast, the dynamics of an initially non-spherical capsule occurs at a fixed total area. Changes in shape arise from redistribution of the excess area between different shape modes. The maximum amplitude of a shape mode is attained when all excess area is transferred into that mode. For example, maximal extension along the vorticity axis corresponds to $\varepsilon f_{20}^{max} = \sqrt{\Delta/2}$, and all other shape modes equal to zero.

For small capsule asphericity, we seek a perturbative solution around a sphere:

$$\boldsymbol{v} = \boldsymbol{v}^{\infty} + \boldsymbol{v}^{(0)} + \boldsymbol{v}^{(1)}(f) + \cdots. \tag{3.5}$$

The leading-order velocity field, $\boldsymbol{v}^{(0)}$, describes the flow about a surface-incompressible sphere placed in a shear flow. The term $\boldsymbol{v}^{(1)}$ describes the flow driven by membrane stresses, i.e. relaxation of the deformed capsule back to the unstressed configuration. To solve for the flow, we adopt a basis of fundamental solutions of the Stokes equations in spherical geometry listed in Appendix F,

$$\left.\begin{aligned} \boldsymbol{v}^{ex} &= \sum_{jmq} [c_{jmq}^{\infty} [\boldsymbol{u}_{jmq}^{+}(\boldsymbol{r}) - \boldsymbol{u}_{jmq}^{-}(\boldsymbol{r})] + c_{jmq} \boldsymbol{u}_{jmq}^{-}(\boldsymbol{r})], \\ \boldsymbol{v}^{in} &= \sum_{jmq} c_{jmq} \boldsymbol{u}_{jmq}^{+}(\boldsymbol{r}). \end{aligned}\right\} \tag{3.6}$$

Summation over repeated indices is implied; q takes values 0, 1 and 2. The functions $\boldsymbol{u}_{jmq}^{\pm}$ are vector solid harmonics related to the harmonics in the Lamb solution. With respect to a sphere, $\boldsymbol{u}_{jm2}^{\pm}$ is radial, while $\boldsymbol{u}_{jm0}^{\pm}$ and $\boldsymbol{u}_{jm1}^{\pm}$ are tangential; $\boldsymbol{u}_{jm1}^{\pm}$ is surface-solenoidal ($\nabla_s \cdot \boldsymbol{u}_{jm1}^{\pm} = 0$). The velocity coefficients c_{jmq} are determined from the condition for velocity continuity and the stress balance equations listed in Appendix D. The far-field (imposed) flow is specified by $\boldsymbol{v}^{\infty} = c_{jmq}^{\infty} \boldsymbol{u}_{jmq}^{+}$. The simple shear flow consists of an extensional component, $\boldsymbol{v}_{ext}^{\infty} = (y, x, 0)/2$, which in the spherical harmonics representation is described by

$$c_{2\pm 20}^{\infty} = \mp \mathrm{i} \sqrt{\frac{\pi}{5}} \quad c_{2\pm 22}^{\infty} = \mp \mathrm{i} \sqrt{\frac{2\pi}{15}}, \tag{3.7a}$$

and a rotational component, $\boldsymbol{u}_{rot}^{\infty} = \frac{1}{2}(y, -x, 0)$, which is specified by

$$c_{101}^{\infty} = -\mathrm{i} \sqrt{\frac{2\pi}{3}}. \tag{3.7b}$$

https://doi.org/10.1017/jfm.2011.108 Published online by Cambridge University Press

The displacement of a material point is also represented in terms of vector spherical harmonics $\boldsymbol{y}_{jmq}$ (E 3)

$$\boldsymbol{d} = \varepsilon \sum_{jmq} d_{jmq} \boldsymbol{y}_{jmq}. \tag{3.8}$$

We see that the displacement vector consists of three components: one radial ($d_{jm2}\boldsymbol{y}_{jm2}$), and two tangential to a sphere ($d_{jm1}\boldsymbol{y}_{jm1}$ and $d_{jm0}\boldsymbol{y}_{jm0}$). The condition for surface-incompressibility at leading order relates two of the displacement amplitudes:

$$\nabla_s \cdot \boldsymbol{d} = 2 f_{jm} - \sqrt{j(j+1)} d_{jm0} = 0, \tag{3.9}$$

where we have taken into account that $d_{jm2} \equiv f_{jm}$, see (3.1). The $\boldsymbol{y}_{jm1}$ vector field is solenoidal and its divergence vanishes identically. Without loss of generality, d_{jm1} can be set to zero at leading order since it is not affected by the rotational component of the imposed shear flow. Hence, to describe the displacement of a material particle, it is sufficient to determine its radial component. The latter is found from the kinematic condition, which at leading order reads

$$\varepsilon \frac{\partial f}{\partial t} = \boldsymbol{v}^{mm} \cdot (\hat{\boldsymbol{r}} - \varepsilon \nabla f). \tag{3.10}$$

The details of the solution are rather technical, and the interested reader can find them in Appendix D. The main result is the evolution equation for the ellipsoidal capsule shape:

$$\frac{\partial f_{2m}}{\partial t} = -\mathrm{i}\frac{m}{2} \Lambda^{-1} \delta_{|m|2} + \mathrm{i}\frac{m}{2} f_{2m} - \Lambda^{-1} \sqrt{\frac{\Delta}{30\pi}} [3\mathscr{B}^{-1}(6+\sigma_0) f_{2m} + 2Ca^{-1}(f_{2m} - g_{2m})]. \tag{3.11}$$

Higher order shape modes ($j > 2$) can be excited by a wrinkling instability under strong compressive strain (Walter *et al.* 2001; Kantsler, Segre & Steinberg 2007) as explained by (Lac *et al.* 2004; Finken & Seifert 2006; Turitsyn & Vergeles 2008). In our analysis, we assume sufficiently weak flows so that membrane buckling does not occur.

In (3.11) σ_0 is the isotropic part of the tension, g_{2m} describe the unstressed configuration, $\delta_{|m|2}$ is the Kronecker delta function and

$$\Lambda = \frac{\sqrt{\Delta}(23\lambda + 32)}{8\sqrt{30\pi}}. \tag{3.12}$$

For comparison, the shape evolution equations for an area-compressible capsule are listed in Appendix H. Shear surface viscosity can be included in a straightforward manner (Lebedev, Turitsyn & Vergeles 2008) by replacing the viscosity ratio with $\lambda \to \lambda + (16/23)\lambda_s$, where λ_s is the dimensionless surface viscosity. The area constraint (3.3) implies $f_{2m}(\partial f_{2m}/\partial t) = 0$ and serves to determine the isotropic part of the tension

$$\sigma_0 = -6 + \mathrm{i}\mathscr{B}\sqrt{\frac{5\pi}{6\Delta}}(f_{22} - f_{2-2}) + \frac{1}{3} Ca^{-1}\mathscr{B}[-2 + g_{20} f_{20} + g_{22} f_{2-2} + g_{2-2} f_{22}]. \tag{3.13}$$

Substituting the above expression in (3.11) leads to a set of nonlinear evolution equations for the shape modes, see (B 1)–(B 4) in Appendix B.

The unstressed shape is assumed to coincide with the initial capsule configuration, and it is specified by

$$r(t=0) = 1 + g_{jm} Y_{jm}(\theta, \varphi). \tag{3.14}$$

https://doi.org/10.1017/jfm.2011.108 Published online by Cambridge University Press

The linear elastic relaxation due to strained current configuration is proportional to the displacement of a material particle from its unstressed configuration, $f_{jm} - g_{jm}$. As explained by Barthes-Biesel & Rallison (1981), since solid body rotation of the membrane does not generate deformation and elastic force, it has to be subtracted from the displacement. Membrane distortion is measured relative to a rotating frame of reference. In general, the rate of rotation is determined as part of the solution (Barthes-Biesel & Rallison 1981). However, at leading order only the solid body rotation by the imposed flow is operative (the capsule dynamics feeds back to the flow and modifies the rotation rate at next order); hence,

$$\frac{\partial g_{jm}}{\partial t} = \mathrm{i}\frac{m}{2} g_{jm}. \tag{3.15}$$

To put our study in the context of earlier work, in the next two subsections we summarize the main analytical results from capsule and vesicle dynamics.

3.1. *Elastic membranes: artificial capsules*

Synthetic capsules have been extensively studied by the group of Barthes-Biesel. However, all analytical work is limited to initially spherical capsules with no bending resistance. By setting $g_{2m} = 0$ and neglecting the bending stresses, (3.11) reduces to (5.6) in Barthes-Biesel & Rallison (1981). The shape evolution equation is linear and does not predict transition to TB:

$$\frac{\partial f_{2m}}{\partial t} = -\mathrm{i}\frac{m}{2}\Lambda^{-1}\delta_{|m|2} + \mathrm{i}\frac{m}{2} f_{2m} - Ca^{-1}\frac{16}{23\lambda + 32} f_{2m}. \tag{3.16}$$

3.2. *Fluid membranes: vesicles*

Setting $Ca^{-1} = 0$ and inserting (3.13) in (3.11) recovers the limit of area-incompressible fluid membranes. Enforcing that area is conserved exactly renders the dynamics nonlinear even at leading order, in contrast to droplets and initially spherical capsules (Misbah 2006; Danker *et al.* 2007; Vlahovska & Gracia 2007; Lebedev *et al.* 2008; Kaoui, Farutin & Misbah 2009; Schwalbe, Vlahovska & Miksis 2010):

$$\frac{\partial f_{2m}}{\partial t} = -\mathrm{i}\frac{m}{2}\Lambda^{-1}\delta_{|m|2} + \mathrm{i}\frac{m}{2} f_{2m} - \frac{1}{2}\Lambda^{-1}(f_{22} - f_{2-2}) f_{2m}. \tag{3.17}$$

The f_{20} and $f_{2\pm1}$ are slaved to the $f_{2\pm2}$ modes, which are excited by the imposed shear. Without loss of generality, we set $f_{2\pm1} = 0$; the $f_{2\pm1}$ modes describe deformations out of the shear plane, which are qualitatively captured by keeping only the f_{20} mode. In this case the evolution equations (3.17) are used to determine $f_{2\pm2}$, while f_{20} is determined from the area constraint (3.3):

$$f_{20} = [2(1 - f_{22} f_{2-2})]^{1/2} = [2(1 - R^2)]^{1/2}. \tag{3.18}$$

Instead of shape modes, the vesicle dynamics can also be described in terms of the orientation angle, ψ, and R, which measures the ellipticity of the vesicle contour in the x–y plane (Misbah 2006):

$$f_{2\pm2} = R\exp(\mp 2\mathrm{i}\psi). \tag{3.19}$$

The evolution equations for the shape and orientation of a fluid membrane vesicle in a simple shear flow are (Misbah 2006)

$$\frac{\partial \psi}{\partial t} = -\frac{1}{2} + \frac{\Lambda^{-1}}{2R}\cos(2\psi), \tag{3.20}$$

https://doi.org/10.1017/jfm.2011.108 Published online by Cambridge University Press

$$\frac{\partial R}{\partial t} = \Lambda^{-1}(1 - R^2)\sin(2\psi). \tag{3.21}$$

This set of coupled nonlinear equations has a stable fixed point corresponding to the TT state ($R^* = 1,\ \psi^* = 1/2 \arccos \Lambda$) and a closed orbit centred at ($\psi^* = 0,\ \ R^* = \Lambda^{-1}$) describing the vacillating-breathing mode (VB), also called trembling (Kantsler & Steinberg 2006) and SW (Noguchi & Gompper 2007). In this motion, the mean inclination angle of the vesicle oscillates between $\pm\pi/4$ and the vesicle shape undergoes large deformations along the vorticity axis. TB corresponds to no equilibrium point. The TT fixed point loses stability at a critical viscosity ratio

$$\lambda_c = -\frac{32}{23} + \frac{120}{23}\sqrt{\frac{2\pi}{15\Delta}}. \tag{3.22}$$

The TB and VB modes coexist within the leading-order theory (Lebedev *et al.* 2008; Kaoui *et al.* 2009), and the mode selection is determined by the initial conditions: if $f_{20} = 0$ the transition is from TT to TB, while if $f_{20} \neq 0$ the transition is from TT to VB.

If there is no deformation along the vorticity direction, i.e. $f_{20} = 0$ at all times, (3.18) implies that R remains constant and is equal to its maximum value 1. This situation resembles the Keller–Skalak model: the vesicle shape is a fixed ellipsoid and the vesicle dynamics is described only by the variations of the angle ψ (note, however, that unlike the Keller–Skalak solution, our velocity field is strictly area-incompressible). In this case the bifurcation is from TT to TB.

If $f_{20} \neq 0$, the transition is from TT to VB. In the breathing (VB) mode, the vesicle undergoes periodic shape deformations along the vorticity direction. As a result, the vesicle appears to tremble in the flow direction.

3.3. *Area-incompressible non-spherical microcapsule*

Finally, by inserting (3.13) into (3.11), we obtain a set of nonlinear equations describing the dynamics of a deformable initially non-spherical microcapsule:

$$\frac{\partial \psi}{\partial t} = -\frac{1}{2} + \frac{\Lambda^{-1}}{2R}\cos(2\psi) + \epsilon_0\frac{(S\Lambda)^{-1}}{2R}\sin(2\phi - 2\psi), \tag{3.23}$$

$$\frac{\partial R}{\partial t} = \Lambda^{-1}(1 - R^2)\sin(2\psi) + (S\Lambda)^{-1}\{\epsilon_0(1 - R^2)\cos(2\phi - 2\psi) - R\sqrt{(1 - R^2)\left(1 - \epsilon_0^2\right)}\}, \tag{3.24}$$

where in order to facilitate comparison with other works (Finken, Kessler & Seifert 2010), we have adopted the notation

$$S^{-1} = \sqrt{\frac{2\Delta}{15\pi}}Ca^{-1}. \tag{3.25}$$

The TT frequency is

$$\frac{\partial \phi}{\partial t} = -\frac{1}{2}, \tag{3.26}$$

where ϕ is the angle between the position vector of a material particle and the flow direction. The SW motion corresponds to a limit cycle of evolution equations (3.23) and (3.24). Increasing the viscosity ratio or shear rate causes the limit cycle to disappear in favour of TB. More details are given in Appendix G.

https://doi.org/10.1017/jfm.2011.108 Published online by Cambridge University Press

The unstressed shape is defined as

$$g_{2\pm2}(t=0) = \epsilon_0 \exp(\mp 2\mathrm{i}\psi_0). \tag{3.27}$$

It does not necessarily have the same excess area as the real shape. For example, if $\epsilon_0 = 0$ and $g_{20} = 0$, the unstressed capsule shape is a sphere. In this case, the evolution equations become independent of the shear elasticity, similarly to the way bending elasticity scales out from the evolution equations for the vesicle dynamics (Olla 2000).

In this study we assume that the unstressed and initial shapes coincide. Hence, the unstressed and current shapes have the same excess area and $g_{20}^2 + 2\epsilon_0^2 = 2$. If $\epsilon_0 = 1$, all excess area is in the $g_{2\pm2}$ shape modes and $g_{20} = 0$. In this case, the capsule contour in the x–y plane remains constant and our model reduces to the Skotheim & Secomb (2007) one, see § 3.3.1. An interesting special case is $\epsilon_0 = 0$, which is considered in § 3.3.2. In the general case $0 < \epsilon_0 < 1$, the initial capsule contour in either the x–z or y–z planes is an ellipse, i.e. the capsule is stretched (or compressed) along the vorticity axis and $g_{20} \neq 0$. Under such circumstances, the capsule exhibits three types of dynamics: SW around a non-zero inclination angle with negligible shape variations (rocking), SW around a nearly zero inclination angle accompanied by large shape oscillations (breathing) and TB. These motions are examined in detail in § 4.

3.3.1. *Fixed-shape ellipsoidal capsule: the Skotheim & Secomb (2007) model*

The evolution equations (3.23) and (3.24) reduce to the shape-preserving model of Skotheim & Secomb (2007), if there is no out-of-the-shear-plane (along the vorticity direction) deformations, $f_{20} = \text{const}$. Because the evolution of the f_{20} mode is slaved to the 2 ± 2 modes, see (B 1), this condition can be strictly enforced only if $f_{20} = 0$ and $g_{20} = 0$, which implies $\epsilon_0 = 1$. In this case, the ellipticity of the vesicle contour remains constant

$$R(t) = 1. \tag{3.28}$$

The capsule dynamics is described by only one variable, the inclination angle ψ and the capsule shape is an ellipsoid whose major axis lies in the plane perpendicular to the undisturbed vorticity. Figure 2 illustrates the angle evolution for a capsule with fixed shape ($\epsilon_0 = 1$) for various viscosity ratios. Figure 2(d) shows the dramatically different behaviour of a capsule with $\epsilon_0 = 0.9999$; this dynamics will be analysed in more detail in § 4.

3.3.2. *Capsule which is initially an ellipsoid with major axis along the vorticity direction*

If $\epsilon_0 = 0$, the shape mode along the vorticity direction contains all excess area and $g_{20} = \sqrt{2}$. In this special case, the capsule never tumbles and always attains a stationary TT state.

The evolution equations (3.23) and (3.24) become autonomous:

$$\dot{\psi} = -\frac{1}{2} + \frac{\Lambda^{-1}}{2R}\cos(2\psi), \tag{3.29}$$

$$\dot{R} = \Lambda^{-1}\sqrt{1-R^2}\,[\sqrt{1-R^2}\sin(2\psi) - S^{-1}R], \tag{3.30}$$

where the over dot denotes the time derivative. The system has fixed points at

$$R_\pm^2 = \tfrac{1}{2}(c \pm \sqrt{c^2 - 4\Lambda^{-2}}), \quad \psi_\pm = \tfrac{1}{2}\arccos(\Lambda R_\pm), \tag{3.31}$$

where $c = 1 + \Lambda^{-2} + S^{-2}$. In the vesicle limit, $S^{-1} = 0$, there are two fixed points corresponding the TT state and the VB state. For small elasticity, we find $R_+^2 = 1 +$

https://doi.org/10.1017/jfm.2011.108 Published online by Cambridge University Press

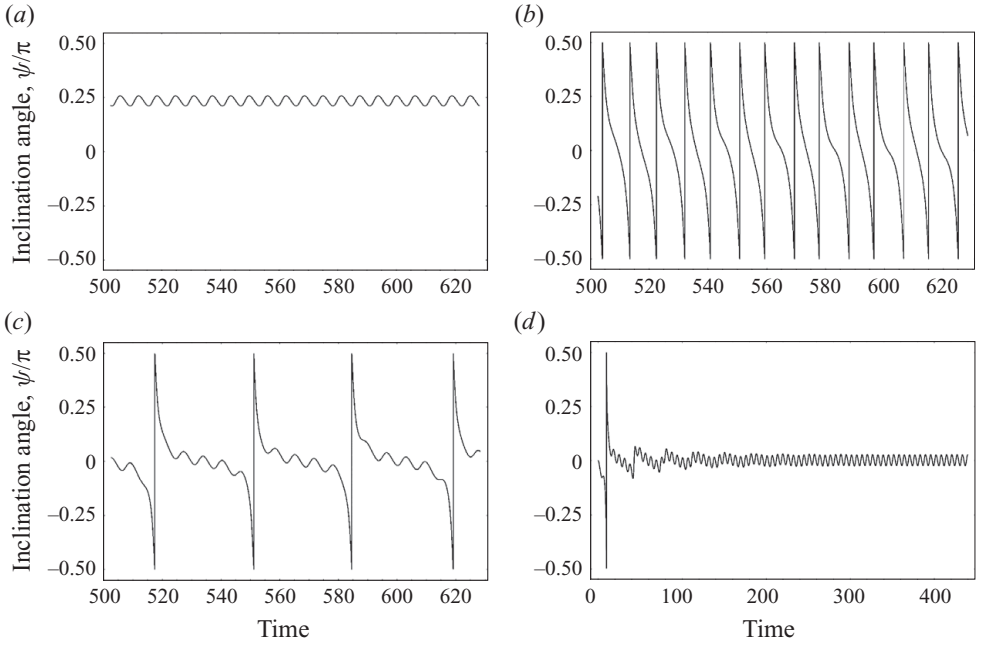


FIGURE 2. Illustration of the SW, TB and intermittent motion of a capsule with excess area $\Delta = 0.02$, asphericity $\epsilon_0 = 1$ and shear rate $Ca = 0.2$. The viscosity ratio is (*a*) $\lambda = 1$ (*b*) $\lambda = 30$ and (*c*) $\lambda = 22.5$. The long-time dynamics is shown after the initial transients have died out. (*d*) Small asphericity in the vorticity direction suppresses the intermittency: the capsule tumbles few times before settling into SW motion. Same parameters as in (*c*) except $\epsilon_0 = 0.9999$.

$S^{-2}(1 + \Lambda^{-2})$ and $R_-^2 = \Lambda^{-1}(1 - \frac{1}{2}S^{-2})$. However, since the maximum value of R is 1, we conclude that R_+ is not physical. In the presence of elasticity, only the VB motion survives. In the rigid ellipsoid limit, $\Lambda^{-1} \to 0$ or $S^{-1} \to \infty$, $R_- = 0$. The capsule has an axisymmetric shape characterized by $\varepsilon f_{20} = \sqrt{\Delta/2}$ and $f_{2\pm2} = 0$ (i.e. the capsule contour in the x–y plane is a circle). The capsule spins around the undisturbed vorticity axis (Jeffrey 1923).

3.3.3. *Weak elasticity*

Let us consider the limit of weak elasticity, $S^{-1} \ll 1$. In this case, the effect of shear elasticity is analysed as a small perturbation around the stationary fixed points corresponding to the TT vesicle, $\psi_{tt} = 1/2 \arccos \Lambda$ and $R_{tt} = 1$, and VB vesicle, $\psi_{vb} = 0$ and $R_{vb} = \Lambda^{-1}$.

Tank-treading state. Introducing $\psi(t) = \psi_{tt} + \Psi(t)$ and $R(t) = R_{tt} + \rho(t)$, and linearizing (3.23) and (3.24) leads to

$$\dot{\Psi} + \Psi\sqrt{\Lambda^{-2} - 1} = \tfrac{1}{2}\epsilon_0 (S\Lambda)^{-1} \sin t, \qquad \dot{\rho} + 2\rho\sqrt{\Lambda^{-2} - 1} = 0. \tag{3.32}$$

At long times, if $\Lambda > 1$, the angle oscillates:

$$\dot{\Psi} + \Psi\sqrt{\Lambda^{-2} - 1} = \tfrac{1}{2}\epsilon_0 (S\Lambda)^{-1} \sin t, \tag{3.33}$$

while at this order the perturbation of shape parameter exponentially decays and the long-time solution for R is time-independent and equal to the value at the stationary point ($R_{tt} \sim 1$). Equation (3.33) can be integrated to give for the long-time 'rocking'

https://doi.org/10.1017/jfm.2011.108 Published online by Cambridge University Press

motion of the capsule:

$$\Psi(t) = \tfrac{1}{2}\epsilon_0 S^{-1}\cos t. \tag{3.34}$$

It shows that the amplitude of the oscillations increases with increasing elasticity or decreasing shear rate. Also, at a given Ca, the amplitude of oscillations is independent of the viscosity ratio.

Vacillating-breathing state. We start from the linearized equation for perturbations (Ψ, ρ), where the angle $\psi = \Psi$ and the amplitude $R = \Lambda^{-1} + \rho$:

$$\left.\begin{aligned} \dot{\Psi} &= -\frac{1}{2}\rho\Lambda - \epsilon_0\frac{S^{-1}}{2}(1-\rho\Lambda)\sin t, \\ \dot{\rho} &= \Lambda^{-1}(1-(\Lambda^{-1}+\rho)^2)\sin(2\Psi) \\ &\quad + (S\Lambda)^{-1}\left[\epsilon_0(1-(\Lambda^{-1}+\rho)^2)\cos(t+2\Psi) - R\sqrt{(1-R^2)\left(1-\epsilon_0^2\right)}\right]. \end{aligned}\right\} \tag{3.35}$$

Taking the time derivative of the first equation, we obtain a harmonic oscillator equation for Ψ as

$$\ddot{\Psi} + (1-\Lambda^{-2})\Psi = -A\cos t + B, \tag{3.36}$$

with

$$A = -\tfrac{1}{2}\epsilon_0 S^{-1}(1-\Lambda^{-2}), \qquad B = \tfrac{1}{2}\Lambda^{-2}S^{-1}\sqrt{(\Lambda^2-1)\left(1-\epsilon_0^2\right)}. \tag{3.37}$$

Equation (3.36) is a forced simple harmonic oscillator with natural frequency $\sqrt{1-\Lambda^{-2}}$ and forcing frequency 1. Therefore, there is no resonance and the perturbation is always oscillating around the mean value ψ_{av}^{vb} obtained from averaging the equation over one period:

$$\psi_{av}^{vb} = \frac{B}{1-\Lambda^{-2}} = \frac{1}{2}S^{-1}\sqrt{\frac{1-\epsilon_0^2}{\Lambda^2-1}}. \tag{3.38}$$

4. Results and discussion

4.1. *Phase diagram of capsule dynamics*

Figures 3 and 4 map capsule dynamics as a function of viscosity ratio, shear rate and asphericity. In order to compare with earlier works by Kessler *et al.* (2008) and Skotheim & Secomb (2007), we have considered an ellipsoid with excess area $\Delta = 0.02$, which corresponds to a prolate ellipsoid with axes 0.9, 0.9 and 1. We have plotted the angle and shape parameter averaged over a period ($T = 2\pi$), as well as the amplitudes of their oscillations:

$$\left.\begin{aligned} \psi_{av} &= \frac{1}{T}\int_0^T \psi(t)\,\mathrm{d}t, \quad R_{av} = \frac{1}{T}\int_0^T R(t)\,\mathrm{d}t, \\ \delta\psi &= \psi_{max} - \psi_{min}, \quad \delta R = R_{max} - R_{min}. \end{aligned}\right\} \tag{4.1}$$

The SW–TB transition is most clearly observed in the amplitude plots – it corresponds to a rapid increase in $\delta\psi$ and a maximum of the shape oscillations δR, see figures 3(b) and 4(c–d).

Capsule dynamics as a function of the viscosity ratio is illustrated in figure 3. We can differentiate three regimes. At low viscosity ratios, the capsule is SW and the inclination angle oscillates around a positive value, see figure 3(c). The average ellipticity R is close to one with negligible oscillations, see figure 3(a); hence, the

https://doi.org/10.1017/jfm.2011.108 Published online by Cambridge University Press

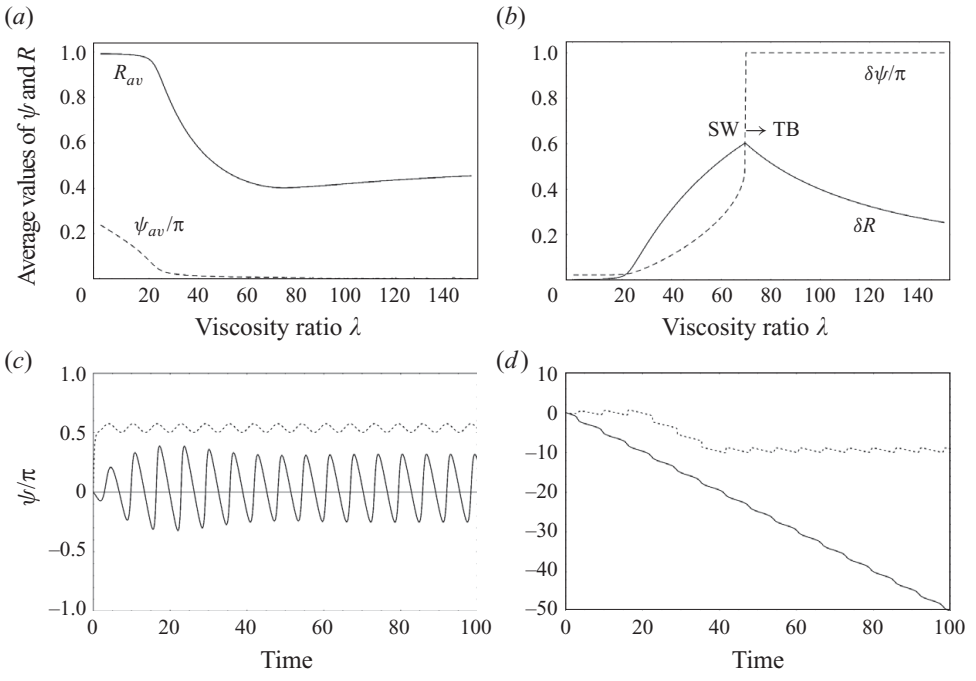


FIGURE 3. (*a*) Dependence on the viscosity ratio of the mean inclination angle ψ_{av} (dashed line) and ellipticity R_{av} (solid line). (*b*) Amplitude of the oscillations of the angle $\delta\psi$ (dashed line) and shape oscillations δR (solid line). The SW–TB transition is marked by jump in $\delta\psi$ and maximal δR. (*c*) Time evolution of the angle for a SW capsule with $\lambda = 10$ (dashed line) and mean inclination angle near zero $\lambda = 50$ (solid line) and (*d*) time evolution of the angle of a capsule in the TB regime $\lambda = 100$ (solid line). The dashed line shows transient 'intermittency' close to the SW–TB transition ($\lambda = 65$). $\epsilon_0 = 0.5$, $Ca = 0.2$ and $\Delta = 0.02$.

capsule shape appears constant. Above a viscosity ratio approximately given by (3.22), the mean inclination angle and R_{av} begin to decrease. The capsule executes breathing motion characterized by strong oscillations in R and a nearly zero average angle. At higher viscosity ratios the capsule tumbles. The TB dynamics is characterized by continuously increasing ψ, illustrated in figure 3(*d*). Near the transition the capsule may also exhibit a transient 'intermittency' – several swings followed by a few tumbles; however, the capsule settles into steady SW. This behaviour is illustrated by the dashed line in figure 3(*d*).

Skotheim & Secomb (2007) first reported that capsules exhibit intermittent behaviour, i.e. SW interrupted periodically by a tumble. However, we find that such intermittent dynamics exists only if $\epsilon_0 = 1$, i.e. initially all excess area is stored in the 2 ± 2 shape modes. For any other value of ϵ_0, the capsule undergoes deformation out of the plane (VB motion) and the intermittency disappears; a capsule may tumble a few times but eventually settles into steady SW motion as seen in figure 3(*d*). Thus, the most important consequence of initial deformation along the vorticity direction ($\epsilon_0 \neq 1$) is that it suppresses the intermittency. It appears that the intermittency is an artefact of the reduced model. Once the full set of (3.23) and (3.24) is solved, no intermittency is observed, only transient TB. This is in agreement with the numerical simulations by Kessler *et al.* (2008), and in contrast to the conclusion by Noguchi (2009) that deformability does not qualitatively change the dynamics. The latter analysis, however, ignores the effect of the tension due to the area constraint.

https://doi.org/10.1017/jfm.2011.108 Published online by Cambridge University Press

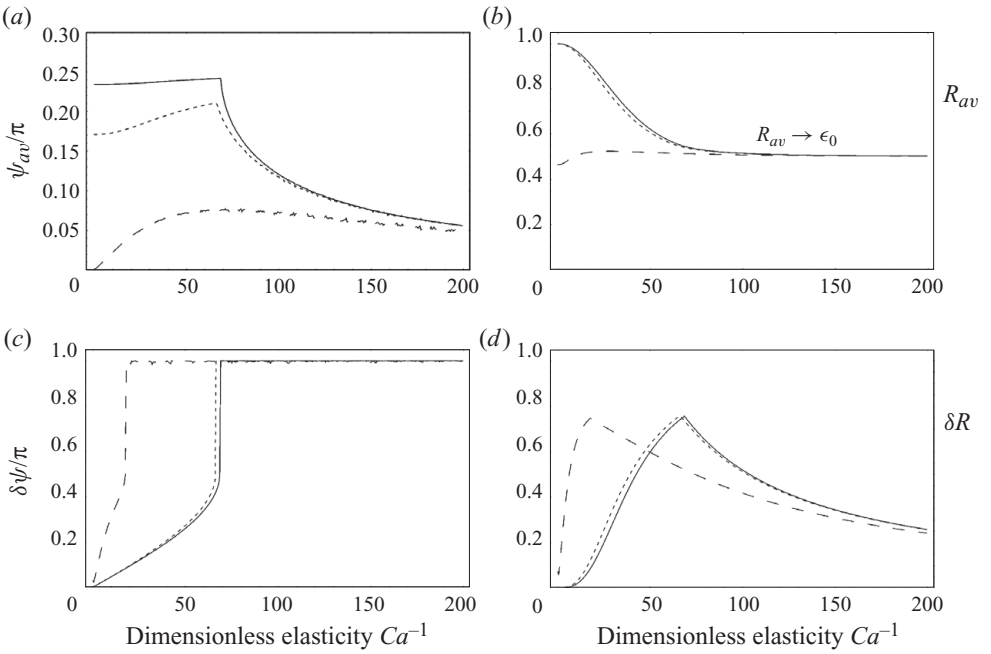


FIGURE 4. Variation with increasing membrane shear elasticity (or decreasing shear rate) of the (a) mean inclination angle ψ_{av}, (b) mean ellipticity R_{av}, (c) amplitude of the angle oscillations $\delta\psi$ and (d) shape oscillations δR. $\epsilon_0 = 0.5$ and $\Delta = 0.02$. Viscosity ratio $\lambda = 1$ (solid line), $\lambda = 10$ (dashed line) and $\lambda = 50$ (long-dashed line). The critical viscosity ratio for the TT–TB transition for a vesicle ($Ca^{-1} = 0$) is 22.5.

Figure 3(a) shows that the mean inclination angle decreases monotonically to zero with viscosity ratio at a given shear rate. However, the variation with the shear rate may not be monotonic, see figure 4(a). The presence of shear elasticity stabilizes the TT state. In figure 4, $\lambda = 50$ is above the critical value for the TT–TB transition of a vesicle (no shear elasticity), and a vesicle tumbles. Under the same conditions, a capsule swings until the shear rate becomes very low; in this case Ca_c is about 0.05. Figure 4(c) also shows that, as predicted by (3.34), in the case $\Lambda < 1$ the amplitude of the oscillations is insensitive to the viscosity ratio.

Finally, the initial asphericity ϵ_0 also affects the transition. Its influence is illustrated on the phase diagrams in figure 5. The points correspond to the SW–TB transition as determined from the jump in $\delta\psi$. Figure 5(b) shows that as $\epsilon_0 \to 0$, the critical elasticity number diverges as $1/\epsilon_0$. Decreasing ϵ_0, which allows for breathing motion along the vorticity direction, widens the SW region, as seen in figure 5(a). This is in agreement with the analysis in §§ 3.3.2 and 3.3.3, which indicated that small non-zero elasticity stabilizes the TT motion.

4.2. *Analysis of the phase boundaries*

From the numerical results shown in figures 3 and 4, we observe that the transition from SW to TB occurs when the instantaneous $R \ll 1$ for small and moderate ϵ_0. However, in the limit of $\epsilon_0 \to 1$, R remains close to unity. In the following we investigate two limits: (i) $0 < \epsilon_0 \ll 1$, $R \sim \epsilon_0$ and (ii) $\epsilon_0 \to 1$ and $R \to 1$.

https://doi.org/10.1017/jfm.2011.108 Published online by Cambridge University Press

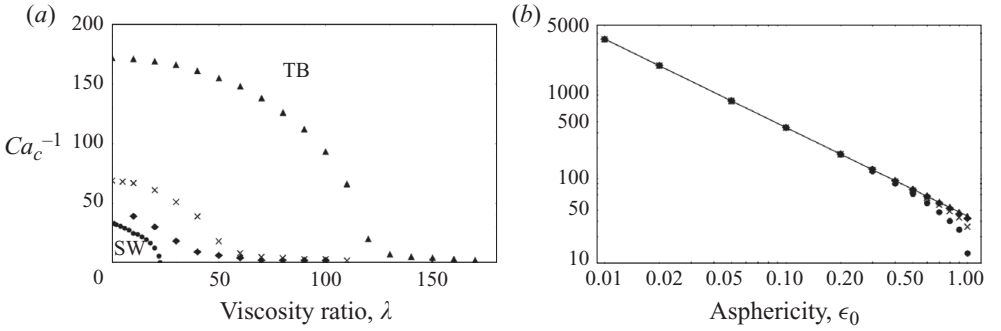


FIGURE 5. Phase boundary between SW and TB for a capsule with $\Delta = 0.02$. (*a*) Critical capillary number as a function of viscosity ratio for different initial non-sphericity along the vorticity direction ϵ: 0.2 (triangles), 0.5 (crosses), 0.8 (diamonds) and 1 (circles). (*b*) Critical capillary number as a function of ϵ_0 for different viscosity ratios $\lambda = 0$ (triangles), $\lambda = 5$ (diamonds), $\lambda = 10$ (crosses) and $\lambda = 20$ (circles). The line is $1/\epsilon_0$.

4.2.1. $0 < \epsilon_0 \ll 1$, $R \sim \epsilon_0$

In this limit (3.24),

$$\dot{R} \sim \Lambda^{-1} \sin(2\psi) + (S\Lambda)^{-1}[\epsilon_0 \cos(t + 2\psi) - R]. \tag{4.2}$$

In this equation, the order 1 quantity is $\rho \equiv R/\epsilon_0$. In terms of ρ,

$$\epsilon_0 \dot{\rho} \sim \Lambda^{-1}(\sin(2\psi) + \epsilon_0 S^{-1}(\cos(t + 2\psi) - \rho)). \tag{4.3}$$

Assuming $\epsilon_0 S^{-1} = O(1)$, we obtain

$$R \sim \epsilon_0 \left[\left(\epsilon_0^{-1} S\right) \sin(2\psi) + \cos(t + 2\psi)\right] \ll 1. \tag{4.4}$$

Equations (4.4) show that R is slaved to the dynamics of ψ in this limit, and ψ can be easily found by integrating

$$\dot{\psi} \sim \tfrac{1}{2}\Lambda^{-1} R^{-1}(\cos 2\psi - \epsilon_0 S^{-1} \sin(t + 2\psi)), \tag{4.5}$$

where R is given by (4.4). The solution is found to depend only on the parameter $\epsilon_0 S^{-1}$. No periodic solution for ψ is found for $\epsilon_0 S^{-1} > 1$, i.e. if $\epsilon_0 S^{-1} > 1$, ψ increases continuously with time, which is a signature of TB, see figure 3(*d*). This implies that the transition from SW to TB occurs at $\epsilon_0 S^{-1} = 1$ for small ϵ_0, i.e.

$$Ca_c^{-1} = \sqrt{\frac{15\pi}{2\Delta}} \epsilon_0^{-1}. \tag{4.6}$$

For small ϵ_0, the critical capillary number Ca_c has no dependence on the viscosity ratio λ and reproduces the transition boundary for $0 \leqslant \epsilon_0 \leqslant 0.5$ in figure 5(*b*) with excellent agreement.

4.2.2. $\epsilon_0 \to 1$ *and* $R \to 1$

When $\epsilon_0 \to 1$,

$$\dot{R} \sim (1 - R^2)(\Lambda^{-1} \sin(2\psi) + (S\Lambda)^{-1} \cos(t + 2\psi)), \tag{4.7}$$

which can easily be integrated to give

$$R(t) = \frac{Ae^{2\int^t \Gamma \, \mathrm{d}t'} - 1}{Ae^{2\int^t \Gamma \, \mathrm{d}t'} + 1}, \tag{4.8}$$

https://doi.org/10.1017/jfm.2011.108 Published online by Cambridge University Press

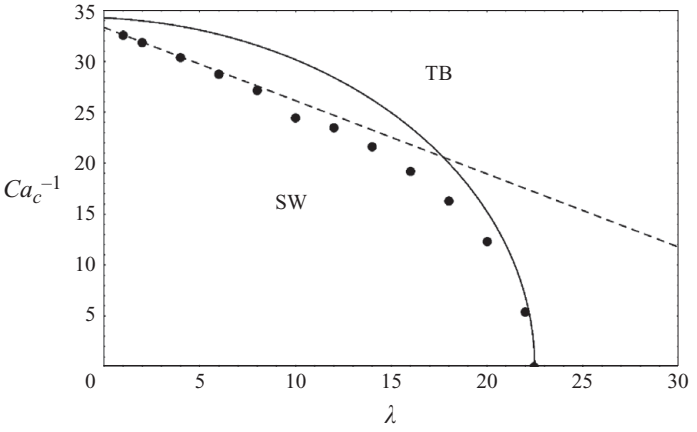


FIGURE 6. Critical elasticity number versus viscosity ratio for $\epsilon_0 = 1$. The points denote transition from SW to intermittent or TB behaviour as determined from the return maps. The solid line is the upper boundary (4.12), $S_c = \sqrt{1-\Lambda^2}$ and the dashed line is the result by Kessler *et al.* (2009), $S_c = 1 - \Lambda/2$.

where $\Gamma \equiv \Lambda^{-1}\sin(2\psi) + (S\Lambda)^{-1}\cos(t+2\psi)$ and A is the integration constant determined from the initial condition. For SW solutions, ψ oscillates around a non-zero value, and therefore $R \to 1$ as time increases. Thus,

$$\begin{aligned}\dot{\psi} &\sim -\frac{1}{2} + \frac{\Lambda^{-1}}{2}\cos(2\psi) - \frac{(S\Lambda)^{-1}}{2}\sin(t+2\psi),\\ &= -\frac{1}{2} + \frac{\Lambda^{-1}}{2}B\cos(2\psi - \theta_B),\end{aligned} \tag{4.9}$$

with

$$B \equiv \sqrt{1 + S^{-2} - 2S^{-1}\sin(t)}, \quad \theta_B \equiv \tan^{-1}\left(\frac{S^{-1}\cos(t)}{1 - S^{-1}\sin(t)}\right). \tag{4.10}$$

At the bifurcation from SW to TB,

$$\int_0^{2\pi} \dot{\psi}\,\mathrm{d}t = \psi(2\pi) - \psi(0) = 0. \tag{4.11}$$

Since $\cos(2\psi - \theta_B)$ is bounded between -1 and $+1$, the integrand, given by (4.9), would be zero if $B = \Lambda$. In order to estimate the critical value of the capillary number Ca_c, we observe that the function $B(S)$ has a minimum when $\sin(t) = \min\{S^{-1}, 1\}$. At the bifurcation, $B_{min} = \Lambda$, which leads to $S_c = \sqrt{1-\Lambda^2}$ (assuming $S > 1$). Hence, the the critical capillary number for transition from SW periodic solution to TB non-periodic solution is

$$Ca_c^{-1} = \sqrt{\frac{15\pi}{2\Delta}}\sqrt{1 - \Delta\left(\frac{(23\lambda + 32)}{8\sqrt{30\pi}}\right)^2}. \tag{4.12}$$

Note that the above derivation also indicates that this boundary should be an upper boundary. Figure 6 shows the phase boundary between SW and TB dynamics.

https://doi.org/10.1017/jfm.2011.108 Published online by Cambridge University Press

5. Conclusions

We have considered the dynamics of a deformable initially non-spherical microcapsule in steady shear flow. We have developed an analytical solution in the asymptotic case where the deformation is limited by small excess area. The theory accounts for the membrane area-incompressibility, resistance to shearing and ellipsoidal unstressed shape. The phase diagram of capsule dynamics is constructed, and analytical results for the phase boundaries are derived. Our results show three regimes of capsule behaviour: rocking, where the main axis oscillates around a positive inclination angle and the capsule shape remains constant, breathing, where the capsule undergoes periodic deformation along the vorticity axis and the mean inclination angle is nearly zero, and TB. Before the transition to TB sometimes transient TB is observed, which in experiments may be mistaken for intermittency if the observation period is too short. Our analysis clarifies the physical basis and limitations of earlier phenomenological models, which are restricted to fixed shape and compressible membrane. In particular, we show that the reported intermittency is an artefact of the shape preservation.

P.M.V. acknowledges partial financial support by NSF grant CBET-0846247. Y.N.Y. thanks Roy Goodman for useful discussions and acknowledges financial support by NSF grants CBET-0853673 and DMS-0708977.

Appendix A. Relation to the work by Kessler *et al*. (2009) and Finken *et al*. (2010)

Finken *et al.* (2010) also analysed the dynamics of a microcapsule in shear flow and independently arrived at similar conclusions to ours. In an earlier paper (Kessler *et al.* 2009), angles Σ and Δ (not to be confused by the excess area in our notation) were employed. They are related to the inclination angle ψ and the TT angle ϕ as follows:

$$\Sigma = -\phi - \frac{\pi}{4}, \quad \Delta = \phi - 2\psi + \frac{\pi}{4}. \tag{A 1}$$

Starting from their equations (21) and (22),

$$\left.\begin{aligned} \partial_\tau \Sigma &= \hat{\lambda} \\ \partial_\tau \Delta &= \hat{\lambda} + 4\sin\Sigma\sin\Delta + 2(\hat{\chi}^{-1} - 1)\cos(\Sigma - \Delta), \end{aligned}\right\} \tag{A 2}$$

we recover our equations (3.23) and (3.24), if we identify λ and χ^{-1} from their notation with

$$\hat{\lambda} \Leftrightarrow \sqrt{\frac{\Delta}{30\pi}}\frac{23\lambda + 32}{8} \equiv \Lambda, \quad \hat{\chi}^{-1} \Leftrightarrow 2\chi\sqrt{\frac{\Delta}{30\pi}} \equiv S. \tag{A 3}$$

Performing the same analysis on (A 2) as in § 4.2 yields the phase boundary reported by Kessler *et al.*, namely

$$\chi_c = \frac{\sqrt{30\pi}}{2\sqrt{\Delta}}\left[1 - \frac{\sqrt{\Delta}}{16\sqrt{30\pi}}(23\lambda + 32)\right]. \tag{A 4}$$

https://doi.org/10.1017/jfm.2011.108 Published online by Cambridge University Press

Appendix B. Shape evolution equations for the deformation of an ellipsoidal particle in shear flow

Ellipsoidal deformation is characterized by only $j=2$ modes. Let us introduce $f_{jm}=f'_{jm}+\mathrm{i}f''_{jm}$ and $f_{j-m}=(-1)^m(f'_{jm}-\mathrm{i}f''_{jm})$, and the same for the g_{jm}.

The shape evolution is described by

$$\frac{\partial f_{20}}{\partial t}=\Lambda^{-1}f_{20}f''_{22}-\frac{1}{2}(S\Lambda)^{-1}[g_{20}(-2+f_{20}^2)+2f_{20}(g'_{22}f'_{22}+g''_{22}f''_{22})] \tag{B 1}$$

$$\frac{\partial f'_{22}}{\partial t}=-f''_{22}+\Lambda^{-1}f'_{22}f''_{22}-\frac{1}{2}(S\Lambda)^{-1}[2g'_{22}(-1+(f'_{22})^2)-f'_{22}(g_{20}f_{20}+2g''_{22}f''_{22})] \tag{B 2}$$

$$\frac{\partial f''_{22}}{\partial t}=-\Lambda^{-1}+f'_{22}+\Lambda^{-1}(f''_{22})^2-\frac{1}{2}(S\Lambda)^{-1}[2g''_{22}(-1+(f''_{22})^2)+f''_{22}(g_{20}f_{20}+2g'_{22}f'_{22})] \tag{B 3}$$

$$\frac{\partial g'_{22}}{\partial t}=-g''_{22}\quad \frac{\partial g''_{22}}{\partial t}=g'_{22}\quad \frac{\partial g_{20}}{\partial t}=0. \tag{B 4}$$

Next we describe the solution.

Appendix C. Formalism

C.1. *Velocity fields and hydrodynamics stresses*

The hydrodynamic tractions exerted on a surface with a normal vector $\boldsymbol{n}$ are $\boldsymbol{n}\cdot\boldsymbol{T}$. They are expanded in vector spherical harmonics (E 3):

$$\boldsymbol{t}\equiv\boldsymbol{n}\cdot\boldsymbol{T}=\tau_{jmq}\boldsymbol{y}_{jmq}. \tag{C 1}$$

In the particular case of a sphere characterized with a normal vector $\hat{\boldsymbol{r}}$, the amplitudes of the viscous tractions and the velocity field are linearly related:

$$\tau^{ex}_{jmq}=\sum_{q'}^{2}c^{\infty}_{jmq'}(\Theta^{+}_{q'q}-\Theta^{-}_{q'q})+\sum_{q'}^{2}c_{jmq'}\Theta^{-}_{q'q} \tag{C 2a}$$

$$\tau^{in}_{jmq}=\sum_{q'}^{2}c_{jmq'}\Theta^{+}_{q'q}, \tag{C 2b}$$

where $\Theta^{\pm}_{q'q}$ are obtained from the velocity fields (F 1)–(F 2) (Bławzdziewicz, Vlahovska & Loewenberg 2000):

$$\Theta^{+}_{qq'}(j)=\begin{pmatrix}2j+1 & 0 & -3\left(\dfrac{j+1}{j}\right)^{1/2}\\ 0 & j-1 & 0\\ -3\left(\dfrac{j+1}{j}\right)^{1/2} & 0 & 2j+1+\dfrac{3}{j}\end{pmatrix} \tag{C 3}$$

$$\Theta^{-}_{qq'}(j)=\begin{pmatrix}-2j-1 & 0 & 3\left(\dfrac{j}{j+1}\right)^{1/2}\\ 0 & -j-2 & 0\\ 3\left(\dfrac{j}{j+1}\right)^{1/2} & 0 & -2j-1-\dfrac{3}{j+1}\end{pmatrix} \tag{C 4}$$

https://doi.org/10.1017/jfm.2011.108 Published online by Cambridge University Press

C.2. *Boundary conditions: stress balance*

The stress balance in terms of spherical harmonics reads

$$\tau^{ex}_{jmq} - \lambda\tau^{in}_{jmq} = \tau^{mm}_{jmq}. \tag{C 5}$$

Tangential stresses correspond to the $q=0, 1$ components, and the normal stresses to $q=2$. The hydrodynamic tractions are given by (C 2). At leading order, the membrane tractions are (Seifert 1999; Olla 2000; Vlahovska & Gracia 2007)

$$\tau^{mm}_{jmq} = \mathscr{B}^{-1}\left(\tau^{\kappa}_{jmq} + \tau^{\sigma}_{jmq}\right) + \tau^{\mu}_{jmq}, \tag{C 6}$$

where the bending stresses are

$$\tau^{\kappa}_{jm2} = j(j+1)(j-1)(j+2)\, f_{jm}, \quad \tau^{\kappa}_{jm0} = 0, \tag{C 7}$$

and the stresses due to membrane tension are

$$\tau^{\sigma}_{jm2} = 2\sigma_{jm} + \sigma_0 (j-1)(j+2)\, f_{jm}, \quad \tau^{\sigma}_{jm0} = -\sqrt{j(j+1)}\sigma_{jm}. \tag{C 8}$$

Note that the membrane tension is non-uniform under non-equilibrium conditions

$$\sigma = \sigma_0 + \sum_{jm} \sigma_{jm} Y_{jm}. \tag{C 9}$$

The surface elastic stresses are

$$\left.\begin{aligned} \tau^{\mu}_{jm0} &= \bar{K}_A\sqrt{j(j+1)}(-2d_{jm2} + \sqrt{j(j+1)}d_{jm0}) + Ca^{-1}(j-1)(j+2)\, d_{jm0}, \\ \tau_{jm1} &= Ca^{-1}(j-1)(j+2)\, d_{jm1}, \\ \tau_{jm2} &= 2\bar{K}_A(2d_{jm2} - \sqrt{j(j+1)}d_{jm0}), \end{aligned}\right\} \tag{C 10}$$

where $\bar{K}_A$ is the dimensionless compression modulus $\bar{K}_A = K_A/\eta_{ex}\dot{\gamma} R_0$.

Appendix D. Solution

D.1. *External flow*

Simple shear flow is defined as

$$\boldsymbol{v}^{\infty} = y\hat{\boldsymbol{x}}, \tag{D 1}$$

which translates into

$$\boldsymbol{v}^{\infty} = \sum_{j=1}^{2}\sum_{m=-j}^{j}\sum_{q=0}^{2} c^{\infty}_{jmq}\boldsymbol{u}^{+}_{jmq} \tag{D 2}$$

$$c^{\infty}_{2\pm 20} = \mp \mathrm{i}\sqrt{\frac{\pi}{5}}, \quad c^{\infty}_{2\pm 22} = \mp \mathrm{i}\sqrt{\frac{2\pi}{15}}, \quad c^{\infty}_{101} = -\mathrm{i}\sqrt{\frac{2\pi}{3}}. \tag{D 3}$$

D.2. *Rotation: tank-treading frequency*

First, we find the velocity field amplitude c_{jm1} using the tangential stress balance with $q=1$:

$$\tau^{ex}_{jm1} - \lambda\tau^{in}_{jm1} = 0. \tag{D 4}$$

This gives

$$c_{jm1} = c^{\infty}_{jm1}\frac{2j+1}{2+j+\lambda(j-1)}. \tag{D 5}$$

https://doi.org/10.1017/jfm.2011.108 Published online by Cambridge University Press

The imposed shear flow (D 3) has a rotational component only with $j=1$, and hence the above relation reduces to

$$c_{101} = c^{\infty}_{101}, \tag{D 6}$$

i.e. the rigid body rotation is unperturbed by the particle, and the particle rotates with the same rate as the flow.

D.3. *Membrane incompressibility*

The local area conservation implies that the velocity field at the interface is solenoidal (Seifert 1999):

$$\nabla_s \cdot \boldsymbol{v} = 0 \quad \text{at} \quad r = 1. \tag{D 7}$$

Therefore, the amplitudes of the velocity field (3.6) are related:

$$c_{jm0} = \frac{2}{\sqrt{j(j+1)}} c_{jm2}. \tag{D 8}$$

D.4. *Tension*

The non-uniform part of the membrane tension, σ_{jm}, is determined from the tangential component of the stress balance (C 5), $q=0$,

$$\sigma_{jm} = \mathscr{B}^{-1}\left[-c^{\infty}_{jm0}\frac{2(1+2j)}{\sqrt{j(j+1)}} + c^{\infty}_{jm2}\frac{3(2j+1)}{j(j+1)} + c_{jm0}\frac{(2+j+\lambda(j-1))}{2\sqrt{j(j+1)}} + 2Ca^{-1}\frac{(j-1)(j+2)}{j(j+1)}(f_{jm}-g_{jm})\right]. \tag{D 9}$$

D.5. *Normal velocity and shape evolution*

The tension (D 9) is substituted into the normal component of the stress balance (C 5), $q=2$, to obtain the normal velocity c_{jm2}:

$$c_{jm2} = C_{jm} - (j+2)(j-1)d(\lambda, j)^{-1}[\mathscr{B}^{-1}(j(j+1)(j(j+1)+\sigma_0))f_{jm} + 4Ca^{-1}(f_{jm}-g_{jm})], \tag{D 10}$$

where

$$C_{jm} = d(\lambda, j)^{-1}[c^{\infty}_{jm0}\sqrt{j(j+1)}\,(2j+1) + c^{\infty}_{jm2}(4j^3+6j^2-4j-3)] \tag{D 11}$$

and

$$d(\lambda, j) = (4+3j^2+2j^3) + (-5+3j^2+2j^3)\lambda. \tag{D 12}$$

Finally, the motion of the interface is determined from the kinematic condition

$$\frac{\partial f_{jm}}{\partial t} = c_{jm2} + \boldsymbol{v}_s \cdot \nabla f \quad \text{at } r=1, \tag{D 13}$$

where $\boldsymbol{v}_s = \boldsymbol{v}^{ex}(r=1) = \boldsymbol{v}^{in}(r=1)$. At leading order, it takes the form

$$\frac{\partial f_{jm}}{\partial t} = c_{jm2} + \mathrm{i}\omega m f_{jm} \quad \text{at } r=1. \tag{D 14}$$

Here, $\omega = 1/2$ is the local rate of rotation. Note that $(\partial/\partial t) - \mathrm{i}\omega m$ is in fact the Jaumann derivative. Substituting c_{jm2} into (D 13) yields the evolution equation for the shape parameters:

$$\frac{\partial f_{jm}}{\partial t} = \mathrm{i}\omega m f_{jm} + C_{jm} + \mathscr{B}^{-1}(\Gamma_1 + \sigma_0\Gamma_2) f_{jm} + Ca^{-1}\Gamma_3(f_{jm}-g_{jm}) + O(\Delta), \tag{D 15}$$

https://doi.org/10.1017/jfm.2011.108 Published online by Cambridge University Press

where

$$\Gamma_1 = -(j+2)(j-1)([j(j+1)]^2)d(\lambda, j)^{-1}, \tag{D 16}$$

$$\Gamma_2 = -(j+2)(j-1)j(j+1)d(\lambda, j)^{-1}, \tag{D 17}$$

$$\Gamma_3 = -4(j+2)(j-1)d(\lambda, j)^{-1}. \tag{D 18}$$

The reference configuration simply rotates with the flow

$$\frac{\partial g_{jm}}{\partial t} = \mathrm{i}\omega m g_{jm}. \tag{D 19}$$

D.6. *Isotropic tension*

The normal velocity (D 10) and the shape evolution (D 15) include the yet unknown isotropic membrane tension. It is expressed in terms of the shape modes and other known parameters in the problem using the area constraint (Vlahovska & Gracia 2007)

$$\Delta = \sum_{jm} a(j) f_{jm} f^*_{jm}, \quad a(j) = \frac{(j+2)(j-1)}{2}. \tag{D 20}$$

Since $\dot{\Delta} = 0$, it follows that

$$\sum a(j) \left(f^*_{jm} \frac{\partial f_{jm}}{\partial t} + f_{jm} \frac{\partial f^*_{jm}}{\partial t} \right) = 0. \tag{D 21}$$

Using (D 15) leads to

$$\sigma_0 = -\frac{\mathscr{B}^{-1}}{\sum_{jm} a(j)\Gamma_2 f_{jm} f^*_{jm}} \sum_{jm} a(j)[C_{jm} f^*_{jm} + \mathscr{B}^{-1}\Gamma_1 f_{jm} f^*_{jm} + Ca^{-1}\Gamma_3(f_{jm} - g_{jm}) f^*_{jm}]. \tag{D 22}$$

In order to clarify the physical significance of the isotropic tension, let us consider the particular case when only the ellipsoidal deformation modes, $j = 2$, are present. Equation (D 9) simplifies to

$$\sigma_0 = -6 + \mathrm{i}\mathscr{B}^{-1}\sqrt{\frac{5\pi}{6\Delta}}\,(f_{22} - f_{2-2}) + \frac{1}{3}\mathscr{B}Ca^{-1}[-2 + g_{20} f_{20} + g_{22} f_{2-2} + g_{2-2} f_{22}]. \tag{D 23}$$

We see that the tension varies with deformation.

Inserting the tension (D 22) into the shape evolution (D 15) and keeping only the $j = 2$ modes yields (B 1)–(B 4).

Appendix E. Spherical harmonics

A good reference on spherical harmonics is Varshalovich, Moskalev & Kheronskii (1988). The normalized spherical scalar harmonics are defined as

$$Y_{jm}(\theta, \varphi) = \left[\frac{2j+1}{4\pi}\frac{(j-m)!}{(j+m)!}\right]^{1/2} (-1)^m P_j^m(\cos\theta)\,\mathrm{e}^{\mathrm{i}m\varphi}, \tag{E 1}$$

where $\hat{\boldsymbol{r}} = \boldsymbol{r}/r$, (r, θ, φ) are the spherical coordinates and $P_j^m(\cos\theta)$ are the Legendre polynomials. For example

$$Y_{10} = \sqrt{\frac{3}{4\pi}}\cos\theta. \tag{E 2}$$

https://doi.org/10.1017/jfm.2011.108 Published online by Cambridge University Press

The vector spherical harmonics are defined as (Bławzdziewicz *et al.* 2000)

$$\left.\begin{aligned} \boldsymbol{y}_{jm0} &= [j\,(j+1)]^{-1/2}\, r\nabla_{\Omega} Y_{jm}, \\ \boldsymbol{y}_{jm2} &= \hat{\boldsymbol{r}} Y_{jm}, \\ \boldsymbol{y}_{jm1} &= -\mathrm{i}\hat{\boldsymbol{r}} \times \boldsymbol{y}_{jm0}, \end{aligned}\right\} \tag{E 3}$$

where ∇_{Ω} denotes the angular part of the gradient operator.

Appendix F. Fundamental set of velocity fields

We reproduce the velocity and stress fields from Vlahovska & Gracia (2007). First we list the expressions for the functions $\boldsymbol{u}^{\pm}_{jmq}(r,\theta,\varphi)$. The velocity field outside the vesicle is described by

$$\boldsymbol{u}^{-}_{jm0} = \tfrac{1}{2} r^{-j}(2-j+jr^{-2})\boldsymbol{y}_{jm0} + \tfrac{1}{2} r^{-j}[j(j+1)]^{1/2}(1-r^{-2})\boldsymbol{y}_{jm2}, \tag{F 1a}$$

$$\boldsymbol{u}^{-}_{jm1} = r^{(-j-1)}\boldsymbol{y}_{jm1}, \tag{F 1b}$$

$$\boldsymbol{u}^{-}_{jm2} = \frac{1}{2} r^{-j}(2-j)\left(\frac{j}{1+j}\right)^{1/2}(1-r^{-2})\boldsymbol{y}_{jm0} + \frac{1}{2} r^{-j}(j+(2-j)r^{-2})\boldsymbol{y}_{jm2}. \tag{F 1c}$$

The velocity field inside the vesicle is described by

$$\boldsymbol{u}^{+}_{jm0} = \tfrac{1}{2} r^{j-1}(-(j+1)+(j+3)r^{2})\boldsymbol{y}_{jm0} - \tfrac{1}{2} r^{j-1}[j(j+1)]^{1/2}(1-r^{2})\boldsymbol{y}_{jm2}, \tag{F 2a}$$

$$\boldsymbol{u}^{+}_{jm1} = r^{j}\boldsymbol{y}_{jm1}, \tag{F 2b}$$

$$\boldsymbol{u}^{+}_{jm2} = \frac{1}{2} r^{j-1}(3+j)\left(\frac{j+1}{j}\right)^{1/2}(1-r^{2})\boldsymbol{y}_{jm0} + \frac{1}{2} r^{j-1}(j+3-(j+1)r^{2})\boldsymbol{y}_{jm2}. \tag{F 2c}$$

On a sphere $r=1$, these velocity fields reduce to the vector spherical harmonics defined by (E 3):

$$\boldsymbol{u}^{\pm}_{jmq} = \boldsymbol{y}_{jmq}. \tag{F 3}$$

Hence, $\boldsymbol{u}^{\pm}_{jm0}$ and $\boldsymbol{u}^{\pm}_{jm1}$ are tangential, and $\boldsymbol{u}^{\pm}_{jm2}$ is normal to a sphere. In addition, $\boldsymbol{u}^{\pm}_{jm0}$ defines an irrotational velocity field.

Appendix G. Some further results illustrating the microcapsule dynamics

Here we provide additional analysis of the microcapsule dynamics and, in particular, the limit cycles.

Figure 7 illustrates the evolution of the limit cycle in the $R-\psi$ phase space. The decreasing radius with increasing ϵ_0 indicates that enhanced deformability along the vorticity direction decreases the amplitude of the oscillations in the x–y plane. Figure 8(a) shows that increasing the elasticity number (decreasing the shear rate) Ca^{-1} increases the amplitude of the oscillations, and eventually causes TB. Finally, figure 8(b) demonstrates that increasing the viscosity ratio λ increases the amplitude of the oscillations.

Examples of the angle evolution are shown in figure 9. At high shear rates (high Ca), the capsule is SW; the inclination angle oscillates around a positive value as shown in figure 9(a). Equation (3.20) has a stable limit cycle as seen in figure 9(b). As the shear rate decreases (Ca decreases), the amplitude of the oscillations increases and

https://doi.org/10.1017/jfm.2011.108 Published online by Cambridge University Press

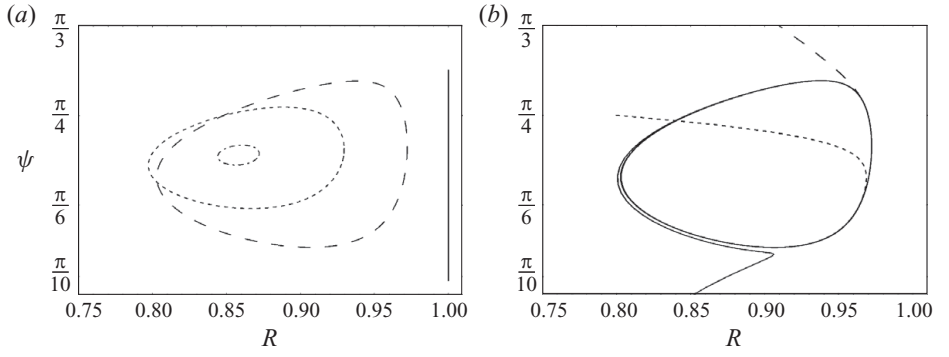


FIGURE 7. (*a*) Effect of the initial non-sphericity along the vorticity direction ϵ_0 on the limit cycle at fixed $Ca^{-1}=20$, $\lambda=5$ and $\Delta=0.02$. $\epsilon_0=$ 1 (solid line), 0.8 (long-dashed line), 0.5 (dashed line) and 0.1 (dot-dashed line). (*b*) The evolution towards the limit cycle for $\epsilon_0=0.8$ with initial conditions $\psi=0$ (solid line), $\pi/4$ (dashed line) and $\pi/2$ (long-dashed line).

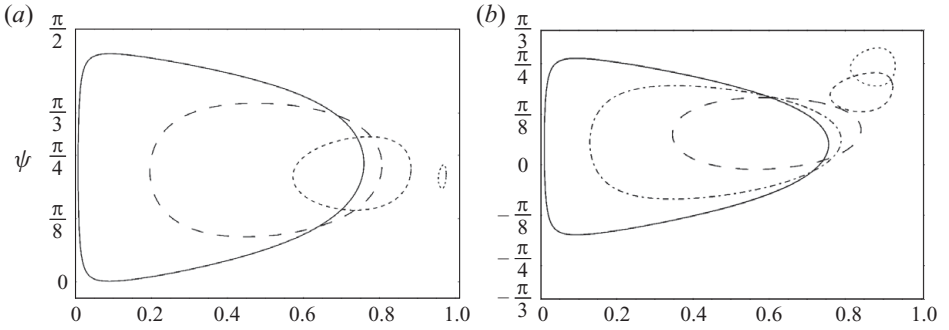


FIGURE 8. (*a*) Effect of Ca on the limit cycle at given $\epsilon_0=0.5$, $\lambda=5$, $\Delta=0.02$. $Ca^{-1}=$ 10 (dotted line), 30 (dashed line), 50 (long-dashed line), 67 (solid line). (*b*) Effect of λ on the limit cycle at given $\epsilon_0=0.5$, $Ca^{-1}=20$, $\Delta=0.02$. $\lambda=$ 0 (dotted line), 10 (dashed line), 30 (long-dashed line), 40 (dot-dashed line) and 48 (solid line).

the radius of the limit cycle also increases. Eventually the limit cycle loses stability and the particle begins to tumble.

Increasing the viscosity ratio, at a fixed elasticity, also causes the limit cycle to disappear in favour of TB because increasing the viscosity ratio decreases the mean inclination angle. However, the SW amplitude is relatively insensitive to the viscosity ratio, as seen in figures 10(*a*) and 10(*b*).

Appendix H. Initially non-spherical area-extensible capsule

For the sake of completeness, here we list the equations for an initially non-spherical capsule with area-compressible membrane:

$$\frac{\partial f_{2m}}{\partial t}=\frac{\mathrm{i}m\sqrt{10\pi/3\Delta}}{(2\lambda+3)}+\mathrm{i}mf_{2m}-4a_1\,(f_{2m}-g_{2m})+2\sqrt{6}\,(a_1+a_2)\,d_{2m0} \tag{H 1}$$

$$a_1=\frac{(\lambda+4)\bar{K}_A}{(3+2\lambda)(16+19\lambda)},\quad a_2=\frac{2(3\lambda+2)Ca^{-1}}{(3+2\lambda)(16+19\lambda)},\quad m=\pm 2 \tag{H 2}$$

https://doi.org/10.1017/jfm.2011.108 Published online by Cambridge University Press

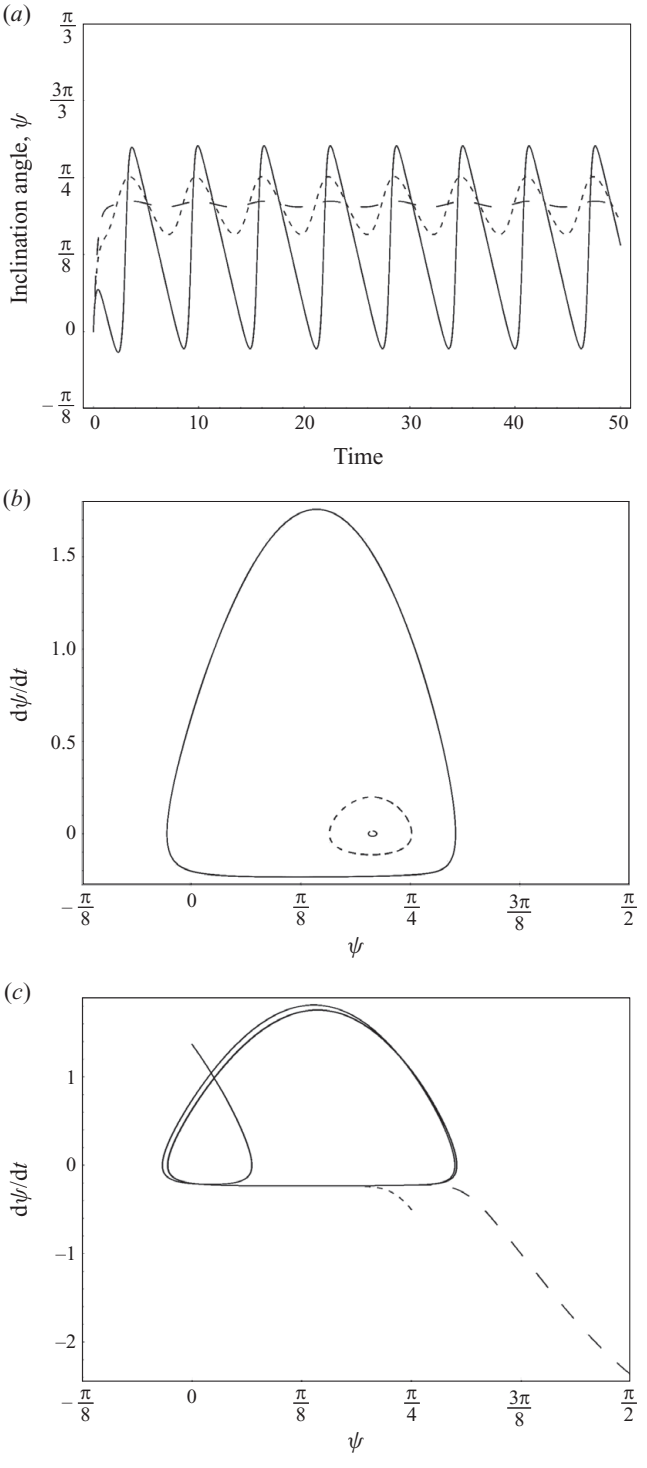


FIGURE 9. SW motion: (*a*) the inclination angle oscillates in time, (*b*) the limit cycle in the phase portrait. The amplitude of the oscillations increases with the elasticity number $Ca^{-1} = 1$ (dotted line) , $Ca^{-1} = 10$ (dashed line) and $Ca^{-1} = 29$ (solid line). The other parameters are $\Delta = 0.02$ and $\lambda = 5$. (*c*) The evolution towards the limit cycle for $Ca^{-1} = 29$ from initial conditions $\psi = 0$ (solid line), $\pi/4$ (dashed line) and $\pi/2$ (long-dashed line).

https://doi.org/10.1017/jfm.2011.108 Published online by Cambridge University Press

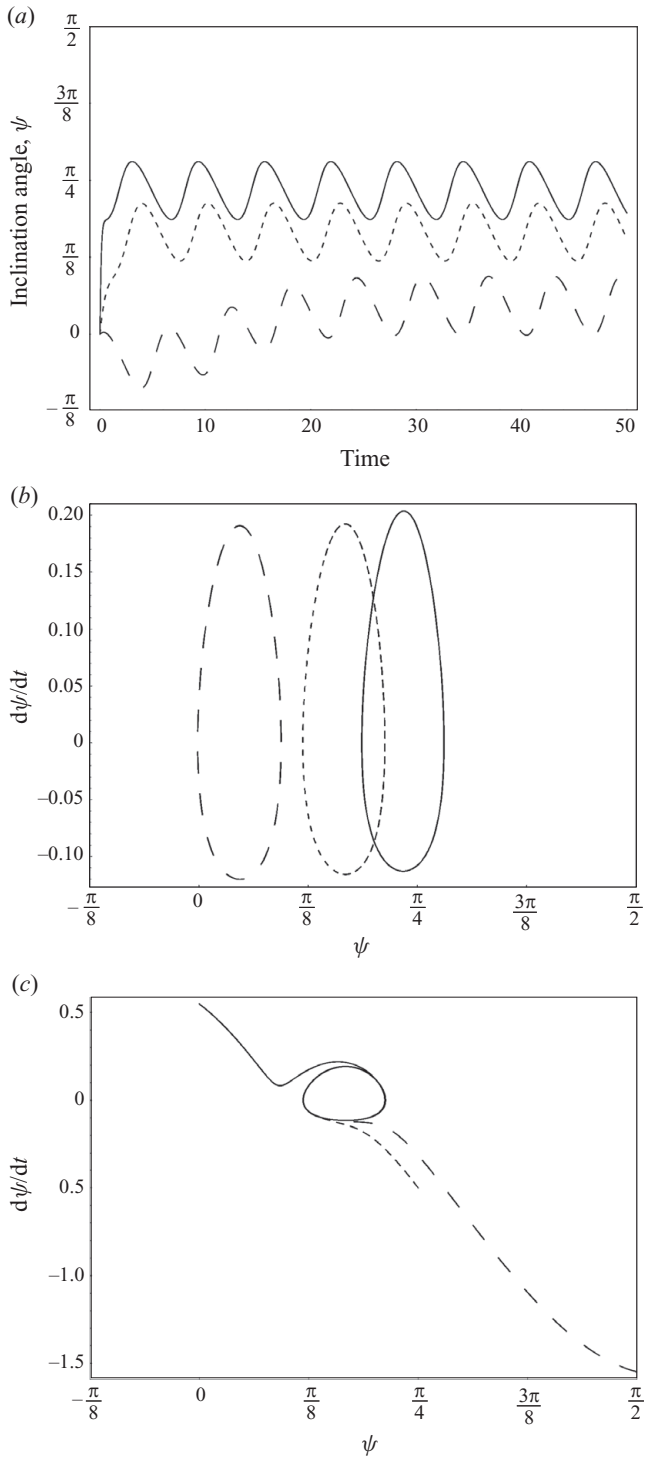


FIGURE 10. Effect of the viscosity ratio on the SW motion. (*a*) Time evolution of the inclination angle. (*b*) Phase portrait. The parameters are $\lambda = 1$ (solid line), $\lambda = 10$ (dashed line) and $\lambda = 20$ (long-dashed line). The excess area is $\Delta = 0.02$ and the elastic capillary number is $Ca^{-1} = 10$. (*c*) The evolution towards the limit cycle for $\lambda = 1$ with initial conditions $\psi = 0$ (solid line line), $\pi/4$ (dashed line line) and $\pi/2$ (long-dashed line).

https://doi.org/10.1017/jfm.2011.108 Published online by Cambridge University Press

$$\frac{\partial d_{2m0}}{\partial t} = \frac{\mathrm{i}m\sqrt{5\pi/\Delta}}{(2\lambda+3)} + \mathrm{i}m d_{2m0} + 2\sqrt{6}b_1\,(f_{2m} - g_{2m}) - 2\,(3b_1 + b_2)\,d_{2m0} \tag{H 3}$$

$$b_1 = \frac{(8+7\lambda)\bar{K}_A}{(3+2\lambda)(16+19\lambda)}, \quad b_2 = \frac{(24+26\lambda)Ca^{-1}}{(3+2\lambda)(16+19\lambda)}. \tag{H 4}$$

REFERENCES

Abkarian, M., Faivre, M. & Viallat, A. 2007 Swinging of red blood cells under shear flow. *Phys. Rev. Lett.* **98**, 188302.

Abkarian, M. & Viallat, A. 2008 Vesicles and red blood cells in shear flow. *Soft Matt.* **4**, 653–657.

Bagchi, P. & Kalluri, R. M. 2009 Dynamics of nonspherical capsules in shear flow. *Phys. Rev.* E **80**, 016307.

Barthes-Biesel, D. 1980 Motion of a spherical microcapsule freely suspended in a linear shear flow. *J. Fluid Mech.* **100**, 831–853.

Barthes-Biesel, D. 1991 Role of interfacial properties on the motion and deformation of capsules in shear flow. *Physica* A **172**, 103–124.

Barthes-Biesel, D. 2010 Capsule motion is flow: deformation and membrane buckling. *Comptes Rendue Phys.* **10**, 764–774.

Barthes-Biesel, D. & Rallison, J. M. 1981 The time-dependent deformation of a capsule freely suspended in a linear shear flow. *J. Fluid Mech.* **113**, 251–267.

Bławzdziewicz, J., Vlahovska, P. & Loewenberg, M. 2000 Rheology of a dilute emulsion of surfactant-covered spherical drops. *Physica* A **276**, 50–80.

Danker, G., Biben, T., Podgorski, T., Verdier, C. & Misbah, C. 2007 Dynamics and rheology of a dilute suspension of vesicles: higher order theory. *Phys. Rev.* E **76**, 041905.

Dimova, R., Aranda, S., Bezlyepkina, N., Nikolov, V., Riske, K. A. & Lipowsky, R. 2006 A practical guide to giant vesicles. Probing the membrane nanoregime via optical microscopy. *J. Phys.: Condens. Matter* **18**, S1151–S1176.

Edwards, D. A., Brenner, H. & Wasan, D. T. 1991 *Interfacial Transport Processes and Rheology*. Butterworth–Heinemann.

Erni, P., Fischer, P. & Windhab, E. 2005 Deformation of single emulsion drops covered with a viscoelastic adsorbed protein layer in simple shear flow. *Appl. Phys. Lett.* **87**, 244104.

Finken, R., Kessler, S. & Seifert, U. 2010 Micro-capsules in shear flow. *arXiv:1004.4879*.

Finken, R. & Seifert, U. 2006 Wrinkling of microcapsules in shear flow. *J. Phys.: Condens. Matter* **18**, L185–L191.

Guido, S. & Tomaiuolo, G. 2009 Microconfined flow behavior of red blood cells in vitro. *Comptes Rendus Phys.* **10**, 751–763.

Helfrich, W. 1973 Elastic properties of lipid bilayers – theory and possible experiments. *Z. Naturforsch.* **28c**, 693–703.

Jeffrey, G. 1923 The motion of ellipsoid particles immersed in a viscous fluid. *Proc. R. Soc. Lond.* A **102**, 169–179.

Kantsler, V., Segre, E. & Steinberg, V. 2007 Vesicle dynamics in time-dependent elongation flow: wrinkling instability. *Phys. Rev. Lett.* **99**, 178102.

Kantsler, V. & Steinberg, V. 2006 Transition to tumbling and two regimes of tumbling motion of a vesicle in shear flow. *Phys. Rev. Lett.* **96**, 036001.

Kaoui, B., Farutin, A. & Misbah, C. 2009 Vesicles under simple shear flow: elucidating the role of relevant control parameters. *Phys. Rev.* E **80**, 061905.

Keller, S. R. & Skalak, R. 1982 Motion of a tank -reading ellipsoidal particle in shear flow. *J. Fluid Mech.* **120**, 27–47.

Kessler, S., Finken, R. & Seifert, U. 2008 Swinging and tumbling of elastic capsules in shear flow. *J. Fluid Mech.* **605**, 207–226.

Kessler, S., Finken, R. & Seifert, U. 2009 Elastic capsules in shear flow: analytical solutions for constant and time-dependent shear rates. *Eur. Phys. J.* E **29**, 399–413.

https://doi.org/10.1017/jfm.2011.108 Published online by Cambridge University Press

Lac, E., Barthes-Biesel, D., Pelekasis, N. & Tsamopolous, J. 2004 Spherical capsules in three-dimensional unbounded stokes flows: effects of membrane constitutive law and onset of buckling. *J. Fluid Mech.* **516**, 303–334.

Lebedev, V. V., Turitsyn, K. S. & Vergeles, S. S. 2008 Nearly spherical vesicles in an external flow. *New J. Phys.* **10**, 043044.

Misbah, C. 2006 Vacillating breathing and tumbling of vesicles under shear flow. *Phys. Rev. Lett.* **96**, 028104.

Navot, Y. 1998 Elastic membranes in viscous shear flow. *Phys. Fluids* **10**, 1819–1833.

Noguchi, H. 2009 Swinging and synchronized rotations of red blood cells in simple shear flow. *Phys. Rev.* E **80**, 021902.

Noguchi, H. & Gompper, G. 2007 Swinging and tumbling of fluid vesicles in shear flow. *Phys. Rev. Lett.* **98**, 128103.

Olla, P. 2000 The behavior of closed inextensible membranes in linear and quadratic shear flows. *Physica* A **278**, 87–106.

Pozrikidis, C. 2003 *Modeling and Simulation of Capsules and Biological Cells*. CRC Press.

Ramanjuan, S. & Pozrikidis, C. 1998 Deformation of liquid capsules enclosed by elastic membranes in shear flow: large deformations and effect of fluid viscosities. *J. Fluid Mech.* **361**, 117–143.

Schwalbe, J., Vlahovska, P. M. & Miksis, M. 2010 Monolayer slip effects on the dynamics of a lipid bilayer vesicle in a viscous flow. *J. Fluid Mech.* **647**, 403–419.

Seifert, U. 1997 Configurations of fluid membranes and vesicles. *Adv. Phys.* **46**, 13–137.

Seifert, U. 1999 Fluid membranes in hydrodynamic flow fields: formalism and an application to fluctuating quasispherical vesicles. *Eur. Phys. J.* B **8**, 405–415.

Skotheim, J. M. & Secomb, T. W. 2007 Red blood cells and other nonspherical capsules in shear flow: oscillatory dynamics and the tank-treading-to-tumbling transition. *Phys. Rev. Lett.* **98**, 078301.

Sui, Y., Chew, Y. T., Roy, P., Cheng, Y. P. & Low, H. T. 2008 Dynamic motion of red blood cells in simple shear flow. *Phys. Fluids* **20**, 112106.

Turitsyn, K. S. & Vergeles, S. S. 2008 Wrinkling of vesicles during transient dynamics in elongational flow. *Phys. Rev. Lett.* **100**, 028103.

Varshalovich, D. A., Moskalev, A. N. & Kheronskii, V. K. 1988 *Quantum Theory of Angular Momentum*. World Scientific.

Vlahovska, P. M. & Gracia, R. 2007 Dynamics of a viscous vesicle in linear flows. *Phys. Rev.* E **75**, 016313.

Vlahovska, P. M., Podgorski, T. & Misbah, C. 2009 Vesicles and red blood cells in flow: from individual dynamics to rheology. *Comptes Rendus Phys.* **10**, 775–789.

Walter, A., Rehage, H. & Leonhard, H. 2001 Shear induced deformation of microcapsules: shape oscillations and membrane folding. *Colloid Surf.* A **183–185**, 123–132.

https://doi.org/10.1017/jfm.2011.108 Published online by Cambridge University Press